
Article:
Sun, X. orcid.org/0000-0001-9035-5523, Mangan, M. orcid.org/0000-0002-0293-8874, Peng, J. et al. (1 more author) (2025) I2Bot: an open-source tool for multi-modal and embodied simulation of insect navigation. Journal of The Royal Society Interface, 22 (222). 20240586. ISSN 1742-5689

https://doi.org/10.1098/rsif.2024.0586

INTERFACE

royalsocietypublishing.org/journal/rsif

Research

Cite this article: Sun X, Mangan M, Peng J, Yue S. 2025 I2Bot: an open-source tool for multi-modal and embodied simulation of insect navigation. *J. R. Soc. Interface* **22**: 20240586.
https://doi.org/10.1098/rsif.2024.0586

Received: 28 August 2024
Accepted: 18 November 2024

Subject Category:
Life Sciences–Engineering interface

Subject Areas:
biomimetics, computational biology, synthetic biology

Keywords:
biorobotics, insect navigation, embodiment, animal intelligence, bio-inspired, insect locomotion

Author for correspondence:
Xuelong Sun
e-mail: xsun@gzhu.edu.cn

Electronic supplementary material is available online at https://doi.org/10.6084/m9.figshare.c.7596418.

THE ROYAL SOCIETY PUBLISHING

I2Bot: an open-source tool for multi-modal and embodied simulation of insect navigation

Xuelong Sun[1,2], Michael Mangan[3], Jigen Peng[1,2] and Shigang Yue[4]

[1]Machine Life and Intelligence Research Center, and [2]School of Mathematics and Information Science, Guangzhou University, Guangzhou, People's Republic of China
[3]Department of Computer Science, Sheffield Robotics, University of Sheffield, Sheffield, UK
[4]School of Computing and Mathematical Sciences, University of Leicester, Leicester, UK

XS, 0000-0001-9035-5523; MM, 0000-0002-0293-8874

Achieving a comprehensive understanding of animal intelligence demands an integrative approach that acknowledges the interplay between an organism's brain, body and environment. Insects, despite their limited computational resources, demonstrate remarkable abilities in navigation. Existing computational models often fall short in faithfully replicating the morphology of real insects and their interactions with the environment, hindering validation and practical application in robotics. To address these gaps, we present I2Bot, a novel simulation tool based on the morphological characteristics of real insects. This tool empowers robotic models with dynamic sensory capabilities, realistic modelling of insect morphology, physical dynamics and sensory capacity. By integrating gait controllers and computational models into I2Bot, we have implemented classical embodied navigation behaviours and revealed some fundamental navigation principles. By open-sourcing I2Bot, we aim to accelerate the understanding of insect intelligence and foster advances in the development of autonomous robotic systems.

1. Introduction

Unravelling the underlying mechanisms that give rise to animal's intelligent behaviours represents a formidable challenge, one that demands an integrative approach that transcends conventional boundaries. Central to this endeavour is the recognition of the dynamic interplay between an organism's brain, body and environment [1,2]—a concept central to the biorobotics approach [3–5]. By bridging the gap between biology and robotics, biorobotics offers a unique opportunity to gain insights into the mechanisms underlying intelligent behaviour [3,6] while simultaneously inspiring the development of more advanced robotic systems [7–9].

Insect navigation stands as a remarkable example of intelligent behaviour, offering a fertile ground for exploration [10]. The intelligence evidenced by insect navigators [11,12] includes both adaptive behaviours that change dynamically as the environment/stimuli changes [13–15] and cognitive behaviours involving complex decision-making and information integration [16–18]. Despite possessing compact neural architectures with limited computational resources, insects demonstrate an astonishing capacity to navigate complex environments [19,20], integrating multi-sensory inputs [16,21], learning from experience [22] and executing adaptive decision-making processes [23–26]. This ability to solve intricate problems with constrained computational power has sparked profound curiosity and a desire to understand the principles that govern these behaviours, with applications possible in AI and robotics [12].

Computational models play an important role in revealing the neural circuits underlying insect navigation [27–29], and some of these models have been verified using mobile robots [28,30,31]. However, these robots could not fully recapitulate the real insects' body due to differences in morphology. Simulations offer significant advantages over real-world robots when studying complex systems, such as the ability to conduct controlled experiments flexibly, modify parameters easily and rapidly iterate through multiple scenarios [32]. Although neuromechanical simulation tools for *Drosophila* have recently been developed [33–35], there remains a lack of tailored, realistic simulation tools for the systematic and comprehensive validation of insect navigation models, particularly for desert ants, that account for physical constraints.

To address these limitations, by leveraging the user-friendly and open-sourced software—***Webots*** [36] (a widely used robot simulation tool in academia [37–40])—we developed a simulation tool that incorporates the morphological characteristics of desert ants, endowing our navigating agent with dynamic vision, olfactory, tactile and mechanosensory capabilities (see figure 1). Leveraging this framework, we have implemented simple forward kinematics (FK) and inverse kinematics (IK) gait controllers, enabling the realization of anatomically constrained computation models for path integration (PI). Additionally, our simulation tool facilitates the integration of vision and olfactory senses, allowing us to explore the sensory-motor closed loop inherent in insect navigation. Through systematic testing, we have uncovered evidence of how body–environment interactions can simplify the design of control models (see table 1). Compared with other related simulation tools, the proposed open-source tool offers advantages in multi-modal sensory capacity, flexibility in constructing three-dimensional (3D) worlds, support for multiple programming languages, lower learning costs and a user-friendly interface (see §4 for more detailed discussion).

By open-sourcing our simulation tool, we aim to provide a valuable resource for the research community, accelerating our collective understanding of insect intelligence. Furthermore, we believe that our work holds significant implications for the development of insect-inspired autonomous robots, offering insights that could pave the way for more adaptive and efficient robotic systems [7,8].

2. Results

Example simulated agent/animal and environments are depicted in figure 1, illustrating the intricate interactions between brain, body and environment. The neural models can be integrated into the *Controller* component of the Webots' Robot. The morphology and spatial configurations of individual organs and limbs are reconstructed based on measurements obtained from real desert ants (refer to §3.1 for detailed information). The environments are assembled using Webots' built-in modules (refer to §3.2 for detailed information).

In this section, we will first introduce the sensory-motor system and the fundamental locomotion capabilities of a simulated desert ant. Following this, as summarized in table 1, we will present several case studies demonstrating the utilization of the proposed tool to implement classical control scenarios in a sensory-motor loop fashion. These simulations provide compelling examples of how I2Bot can offer new insights into understanding insect intelligence through the dynamic interaction between brain, body and environment. In the future, we hope for the tool to be extended to include additional sensory modalities, brain models and body structures of other insects (see §4.2). Note that force sensing (e.g. mechanosensory, tactile) is not utilized in the current implementation of vision- and olfactory-based behaviours. However, the sensory repertoire can be easily extended to incorporate force sensing data from the antennae and legs in specific scenarios, as these capabilities are already available (see figure 1).

2.1. Sensors and motors

Insects rely on multi-modal sensory information to perceive their environment and make decisions [45]. Among these modalities, vision, olfaction and tactile cues are considered crucial for insect navigation. A valuable tool should facilitate easy access to these sensory signals. To address this, the ant robot in I2Bot has been equipped with visual, olfactory and force sensors. As depicted in figure 1, two distinct vision sensors—binocular and panoramic—have been incorporated to serve different purposes in visual processing. Similarly, the proposed tool enables simulation of olfactory signals with various spatio-temporal patterns, such as stable odour trails for simulating trail following and dynamic odour plumes for investigating navigation in turbulent olfactory environments. Tactile and mechanosensory input is simulated through force sensors located at the tip of each leg, the tip of each antenna and torque sensors located in each leg joint (five per leg), at three locations in each antenna, and two in the neck and abdomen joints. Finally, wind sensing is simulated by two sensors positioned at the tip of the antennae, see figure 1 for overview.

The locomotion capabilities of insects have long intrigued researchers and have served as inspiration for the design of six-legged robots [4,8]. To replicate the authentic locomotion of insects, we have defined five degrees of freedom (d.f.) for each leg (i.e. front left, FL; middle left, ML; hind left, HL; front right, FR; middle right, MR; hind right, HR). The joints are designated based on the anatomy of body and leg segments. For instance, the joint ThCz refers to the joint connecting the thorax and coxa, rotating along the z-axis. To streamline body movement, the head and abdomen each possess two d.f., allowing rotation along the y- and z-axes. Recent studies have emphasized the pivotal role of active olfactory sensing [44,46,47] in shaping the navigational behaviours of insects and its application in robotics [48]. Therefore, each antenna of I2Bot is equipped with three d.f. to enable agile movement of the antenna.

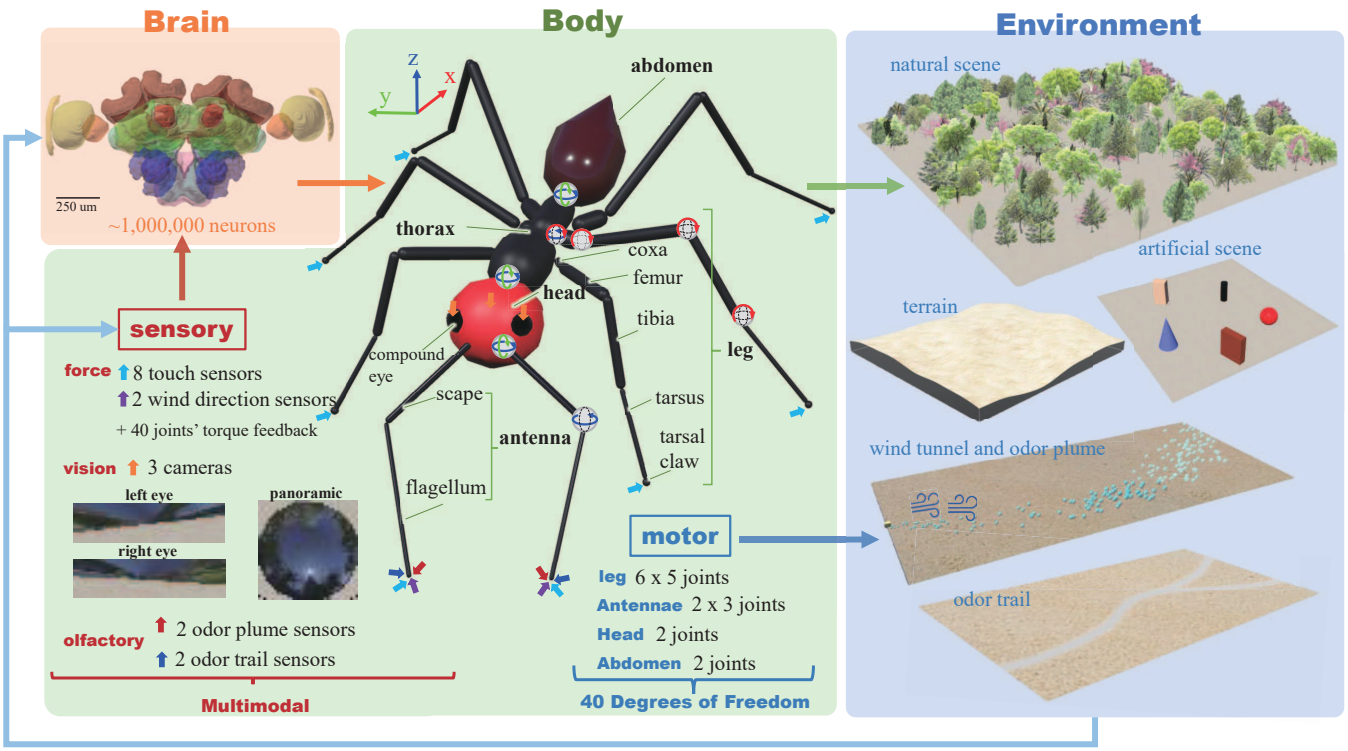

Figure 1. I2Bot overview. The tools aim to integrate simulation of brain, body and environment, encompassing the sensory-motor loop. Colour-coded arrows indicate the positions of corresponding sensors, while joints are identified by their rotation axes. Note data here are for illustrative purposes, with specific examples shown in subsequent figures. Picture of the reconstructed insect brain is obtained from the InsectBrainDB [41].

Table 1. Summary of the presented case studies with I2Bot. Bold text highlights the new insights and contributions.

	sensor	motor	environment
path integration	velocity + direction	six legs	plain terrain
	bio-plausible neural output and simple gait control facilitate homing [28,31]		
visual beacons	binocular/monocular vision	six legs	plain terrain and 3D trees
	embodied sensory input effects the performance of controller [1,2]		
visual compass	panoramic vision	six legs	plain terrain and 3D trees
	How internal representation of direction could control body orientation [42,43]		
odour trail following	odour concentration (stable)	six legs + two antenna	optic-simulated odour trail
	embodied sensors simplify the design of the controller [44]		
odour plume tracking	odour concentration (fluctuated) + wind direction	six legs	virtual wind and odour puffs
	first implementation of the embodied plume tracking [13]		

2.2. Basic locomotion

Locomotion is the basis of complex manoeuvres that have been observed in insects, thus it is crucial for navigation behaviours. To simplify the locomotion control, we have adapted concepts from robotics and implemented a simple gait control algorithm based on forward and inverse kinematics (FK and IK). Unlike higher level locomotion controllers [49,50] wherein the gait is assumed fixed or emergent, this approach concerns the movement of each joint (i.e. directly sets the angle of each joint) for a given leg movement pattern (i.e. a gait); a kind of lower level method without considering the muscles' contraction and relaxation [51]. Specifically, the FK method directly assigns the joint angle which determines the position of the leg tip, while the IK computes each joint angle given the spatial position of the end tip of each leg (for more details see §2.3). That is to say, in FK we design the joint angles, while in IK we design the spatial movement of the leg tip (i.e. design the spatial location of the tip of each leg at every time step), and the corresponding joint angles at every time step are computed through trigonometry-based methods. Note that in the current implementation, we only use three d.f. of each leg (keeping angles of the ThCx and the TiTa joint constant), which is simpler and more usual for hexapod robots. However, users could in practice apply all the five d.f. to replicate more biologically realistic locomotion control. In summary, the locomotion models currently included are based on robot control strategies and could be efficiently upgraded to match models from the biological literature (e.g. [49,52]) since the joint torque feedback are already accessible.

As depicted in figure 2*a,b*, IK-based gait control exhibits greater stability but demands more computational resources. To assess the motion control's performance, we evaluated its ability to navigate uneven terrain and climb walls. Figure 2*c* illustrates the comparison of walking on floors with varying degrees of unevenness. Here, we observed faster changes in the *z*-position of the body with negligible differences in joint torques, indicating the six-legged robot's inherent capacity to navigate uneven terrain embedded in its physical dynamics. In climbing vertical walls, insects utilize adhesion which we simulated by dynamically applying force to the leg's ground contact points. Figure 2*d* presents the climbing performance with varying levels of force applied to the ground support points. Interestingly, larger force does not necessarily translate to better wall-climbing performance. This may be due to the competition between the force required to lift the leg and the force needed to maintain contact with the wall. Different gait types are demonstrated in figure 2*g,h*, with the tripod gait achieving the fastest body movement speed, while the wave tripod is the slowest. It is worth noting that other gait controllers such as central pattern generator (CPG) and feedback models [4,49,53,54] could also be integrated. Here, we present the simple FK-based gait controller to showcase the proposed tool's feasibility.

2.3. Path integration: incorporating locomotion with a bio-constrained neural model

Path integration (PI) stands as a cornerstone of the insect navigation toolkit [55]. Foragers adeptly track the distance and direction to their nest by integrating the series of directions and distances travelled into a *home vector* [19,56]. Guided by this vector, pointing towards the start position (typically the nest), desert ants can return accurately to their nest even after traversing hundreds of metres (figure 3*a*). Recent neuroethological investigations have unveiled the central complex (CX) within the insect brain as pivotal for the computational processes involved in path integration. The CX not only hosts a ring attractor network encoding the animal's heading direction [57,58] but also receives optic flow information as a velocity encoding [28,59].

To demonstrate the ease of incorporating biologically constrained neural models with locomotion controllers using I2Bot, we implemented the popular insect path integration model proposed by Stone *et al.* [28]. We utilized its output as tuning factors for the previously described FK gait controller. Specifically, the neural activation of the left and right PFL/CPU1 neurons from the insect steering circuit modifies the *hip swing* (speed) and *rotation* (direction) of the gait (figure 3*b,c*). This marks the first instance of testing this popular neural model in a hexapod robot with physical constraints and ant-like morphology. Notably, the simulated ant can perform curved walking, unlike a recent biorobotics study [31] where the robot could only rotate on the spot. Several simulations were conducted, and we found that this bio-constrained model performed effectively (see figure 3*d,e*), suggesting a robust and efficient solution for robot path integration. Figure 3*f,g* illustrates the dynamic neural activation of the encoded *home vector* and the agent's velocity during foraging and homing. This exemplifies how neural computation and encoding, coupled with a simple locomotion controller, can generate robust navigation behaviours.

2.4. Vision-guided manoeuvres

Vision serves as one of the primary means for animals to perceive their environment, and insects rely on visual cues for navigation in various ways [60,61]. In this section, we present scenarios involving monocular, binocular and widely used panoramic vision to demonstrate vision-motor control in the simulated ant robot.

2.4.1. Monocular and binocular visual beacons

Research has indicated that insects instinctively use visual landmarks as beacons [62,63]. To showcase the feasibility of using visual images as input with our proposed tool, we implemented a simple visual beacon algorithm (see figure 4*a,b*) based on the biologically plausible steering circuit used in neural models of the insect brain [28,29,59]. To compare the effects of different types of visual input on motor output, we employed monocular (i.e. solely left or right image) and binocular images as inputs to the visual beacon model. The results are illustrated in figure 4*d*, where the simulated ant with binocular image inputs outperforms the others in terms of task completion time. Eye occlusion resulted in ipsilateral motor bias, where agents with the left eye occluded (receiving only right eye information) approached the landmark with left-biased trajectories (red curves in figure 4*c*). This illustrates how embodied sensory input influences navigation performance guided by the same neural controller, providing partial insights into the advantages of binocular vision.

2.4.2. Panoramic visual compass

In addition to binocular vision, insects are believed to use panoramic views when navigating [64–66]. Computational models also leverage panoramic images to extract useful information for solving visual navigation tasks, particularly in the frequency domain [29,67,68]. Here, we demonstrate how processing panoramic views in the frequency domain can aid the agent in sensing direction, known as the visual compass [66,69]. The methods used to process the panoramic view here are the same as those in [29,68], which could also serve as the foundation for insect visual route following behaviour (see figure 5*a*). The initially extracted phase encoding in the frequency domain is stored as the desired heading direction. When the simulated three-dimensional world is manually rotated, the received panoramic image and the phase encoding rotate accordingly. The

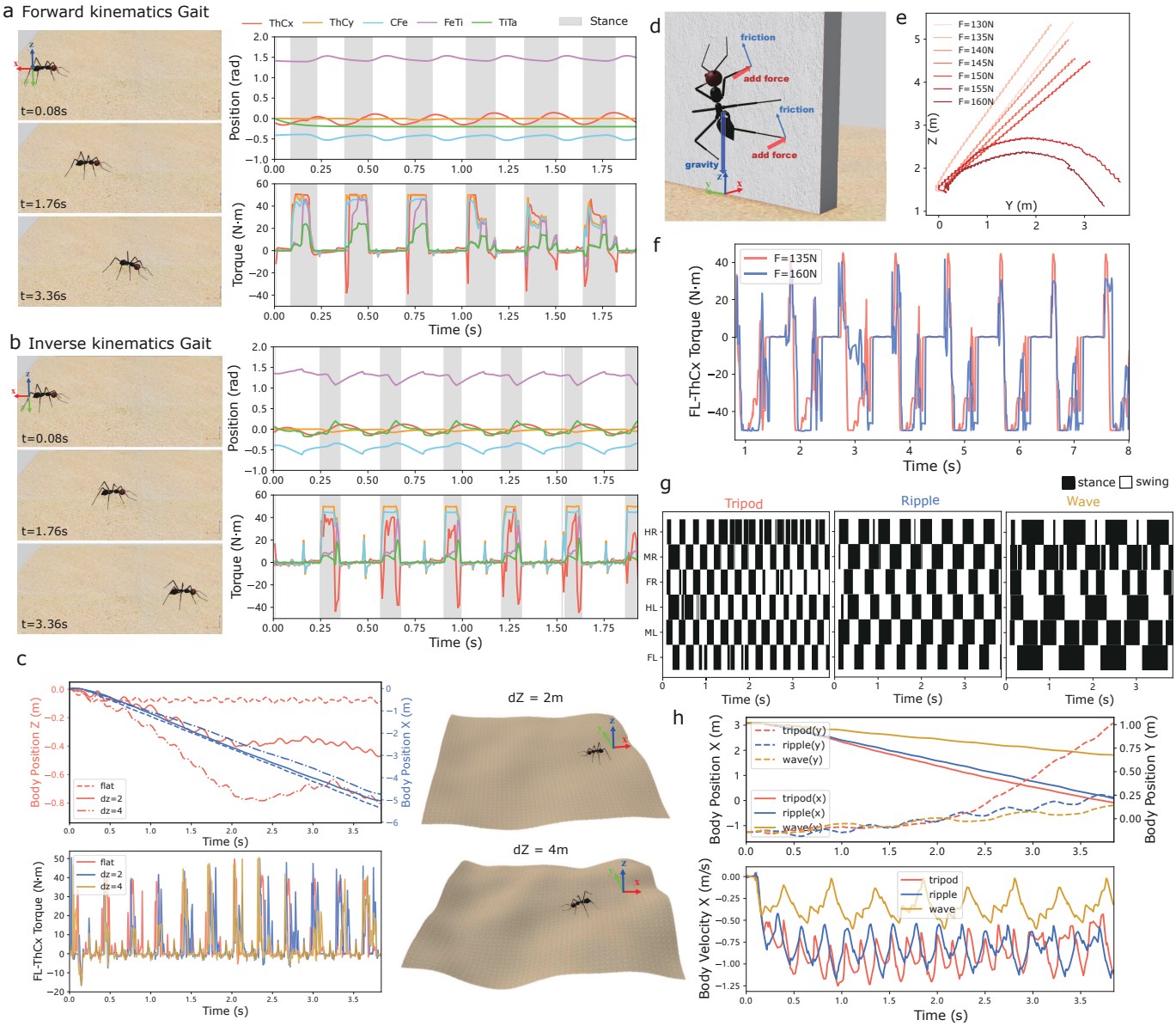

Figure 2. Locomotion and gait control. (*a–b*) Left: snapshots of walking ants at specific times; right: joint position and torque of the middle right leg based on FK and IK. (*c*) Walking on uneven terrain. (*d–f*) Climbing the wall using adhesion with different force added at the tip of each leg, trajectories are shown in (*e*) and the torque values are plotted in (*f*). (*g–h*) FK-based implementation of different gait types: tripod, ripple and wave. Note that when walking on the floor, the robot is initially facing negative *x*-axis (see the coordinates labelled in figure 1). All the origins are marked in the figure for clarification.

difference between the stored phase and the current phase is output to the steering circuit, enabling the agent to turn and continuously maintain its initial heading. To test the performance of the visual compass-based head tracking, we rotated the three-dimensional world in two modes: incremental rotation and jump rotation (sudden and fast). As shown in figure 5*c* and electronic supplementary material, videos S8–S9, the simulated ant efficiently tracked its stored initial heading in both rotation modes, consistently orienting towards the red ball in the three-dimensional visual world.

2.5. Olfactory-guided manoeuvres

Olfaction represents another crucial sensory domain guiding a diverse array of navigational behaviours [13,70–72]. Different olfactory landscapes lead to varied navigation behaviours [73]. To showcase how the proposed platform facilitates olfactory navigation simulation under environments with different spatio-temporal features, we implemented odour trail following behaviour under a spatially stable distribution [74] and odour plume tracking behaviours in a turbulent olfactory environment [13].

2.5.1. Odour trail following using active sensing

Odour trail following [44] observed in carpenter ants (*Camponotus pennsylvanicus*) was realized to demonstrate how embodiment benefits the design of control strategies. We compared the trail following performance of agents with and without moving their antennae during odour tracking by measuring the time taken to navigate from the same start point to the end of the

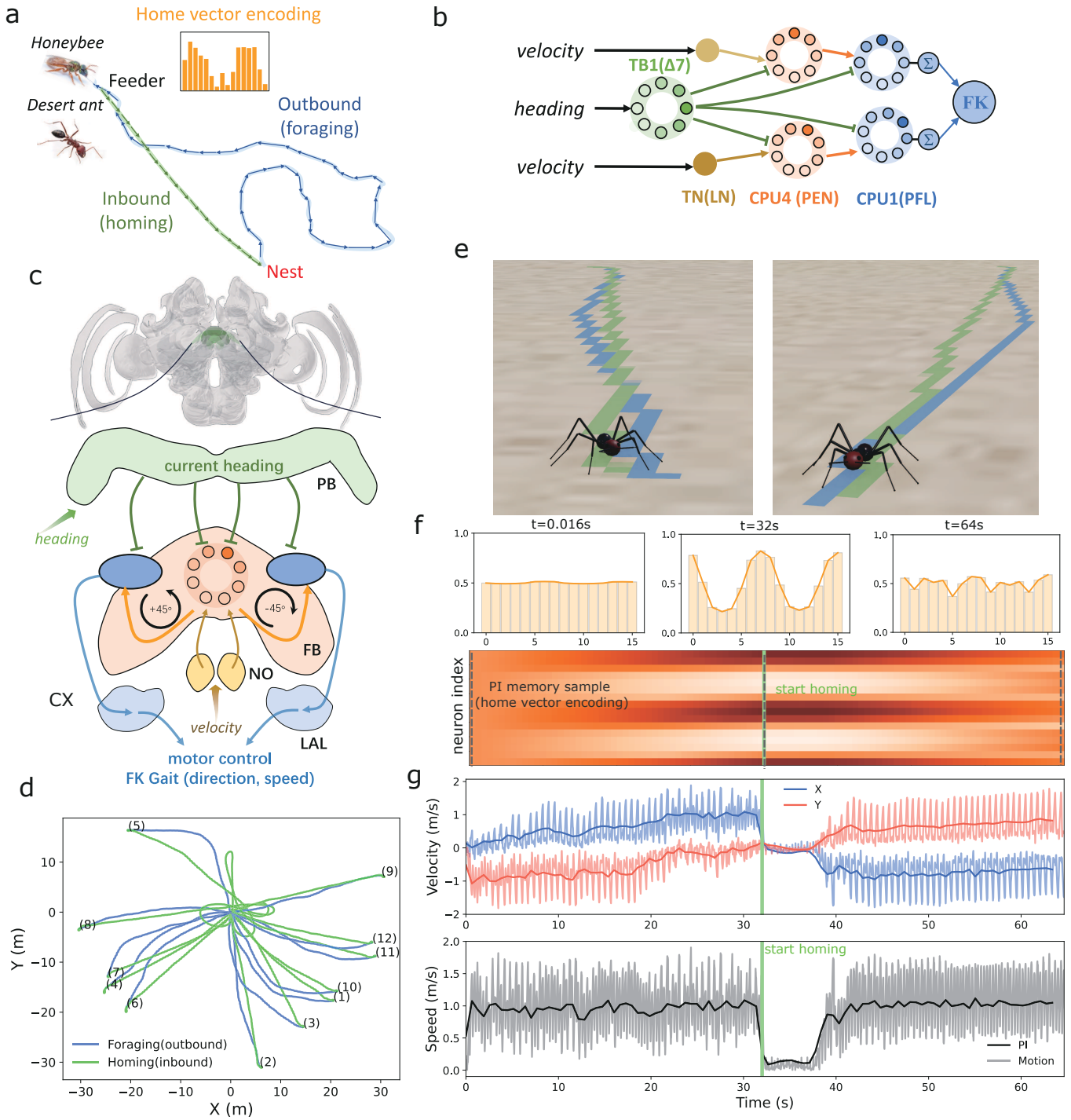

Figure 3. Implementation of path integration model. (*a*) Schematic diagram of central-foraging insects' path integration. Photo of the bee is from A. Narendra; photo of the ant is adapted from https://www.karincadunyasi.com/forum/konu/cataglyphis-nodus.63. (*b*) The neural model of path integration adapted from [28]. The output of the model is linked to the FK gait controller. (*c*) Insect brain regions within the central complex related to PI computation. (*d*) Trajectories of simulated ants conducting foraging trips and homing using the proposed PI model. (*e*) Snapshots of two typical experiments. Trajectories are drawn using the *Pen* function within Webots. (*f*) Neural activation of PI memory neurons (CPU4 or FPN neurons) during foraging and homing, with sampled points marked by grey dotted lines. Corresponding activation profiles are placed above. (*g*) Velocity in the *x*- and *y*-axis (top) and speed (bottom) during navigation. Dark solid lines indicate the inputs fed into the PI model, while lighter curves show instant velocity measurements of the walking robot.

pheromone trail (finish time as shown in figure 6*d*). Intriguingly, we found that agents with moving antennae significantly outperformed those with fixed antennae (figure 6*c*,*d*) when tracking spatially wider trails, although their performance on trails with normal width was similar. This suggests that dynamic antennae movement enhances the adaptability of control strategies to handle a wide range of environmental conditions, as demonstrated in [44]. This finding underscores how embodiment facilitates the design of effective control systems [2].

In addition, I2Bot simplifies body modification. For example, electronic supplementary material, video S12, demonstrates a preliminary test where ant robots with varied antenna lengths, but identical control algorithms, exhibited different performances in odour trail following. This together with the results presented in the visual beacon simulations (figure 4) further

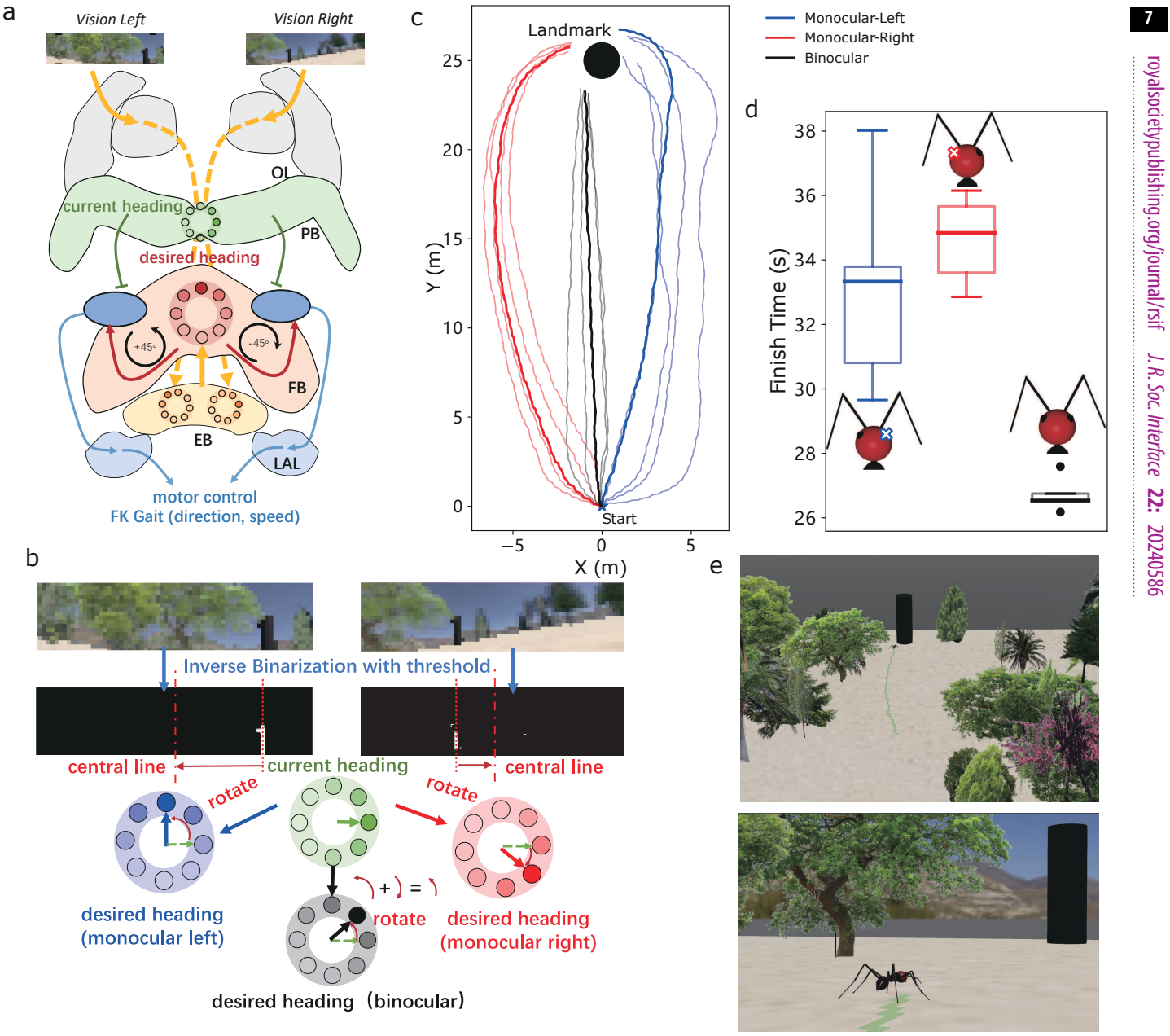

Figure 4. Visual beacons with monocular and binocular vision. (*a*) Schematic diagram of the visual beacons model overlapped with the insect brain regions. (*b*) Illustration of generating the desired heading from the visual inputs with monocular and binocular visual input. (*c*) Trajectories of the visual beacon using left, right and binocular vision. (*d*) Time taken by the robot to reach the position near the landmark. (*e*) Snapshots of the simulated ant robot and environment during visual beacon navigation.

highlights the impact of body morphology and physical dynamics on the development of control algorithms and neural circuitry. It underscores that intelligence develops through the intricate interaction between body, brain and environment [1].

In addition, I2Bot simplifies body modification. For example, electronic supplementary material, video S12 demonstrates a preliminary test where ant robots with varied antenna lengths, but identical control algorithms, exhibited different performances in odour trail following. This together with the results presented in the visual beacon simulations (figure 4) further highlights the impact of body morphology and physical dynamics on the development of control algorithms and neural circuitry. It underscores that intelligence develops through the intricate interaction between body, brain and environment [1].

2.5.2. Odour plume tracking

To investigate sensory-motor control in turbulent odour environments, we developed a simplified control strategy inspired by behaviours observed in walking flies [13]. While this behaviour has been extensively modelled in previous studies [17,75], we adapted a conceptual model to validate the proposed tool's capacity to implement dynamic olfactory navigation behaviours. As illustrated in figure 6*e*, once the odour is sensed (i.e. the perceived odour concentration exceeds the threshold), the agent orients upwind (aligning with the wind direction detected via the virtual mechanosensory signal). In the absence of odour, the agent performs random rotations in place, simulating scanning/searching manoeuvres. Despite discontinuous olfactory and mechanosensory cues in this turbulent environment, agents successfully navigate to the odour source using this simple

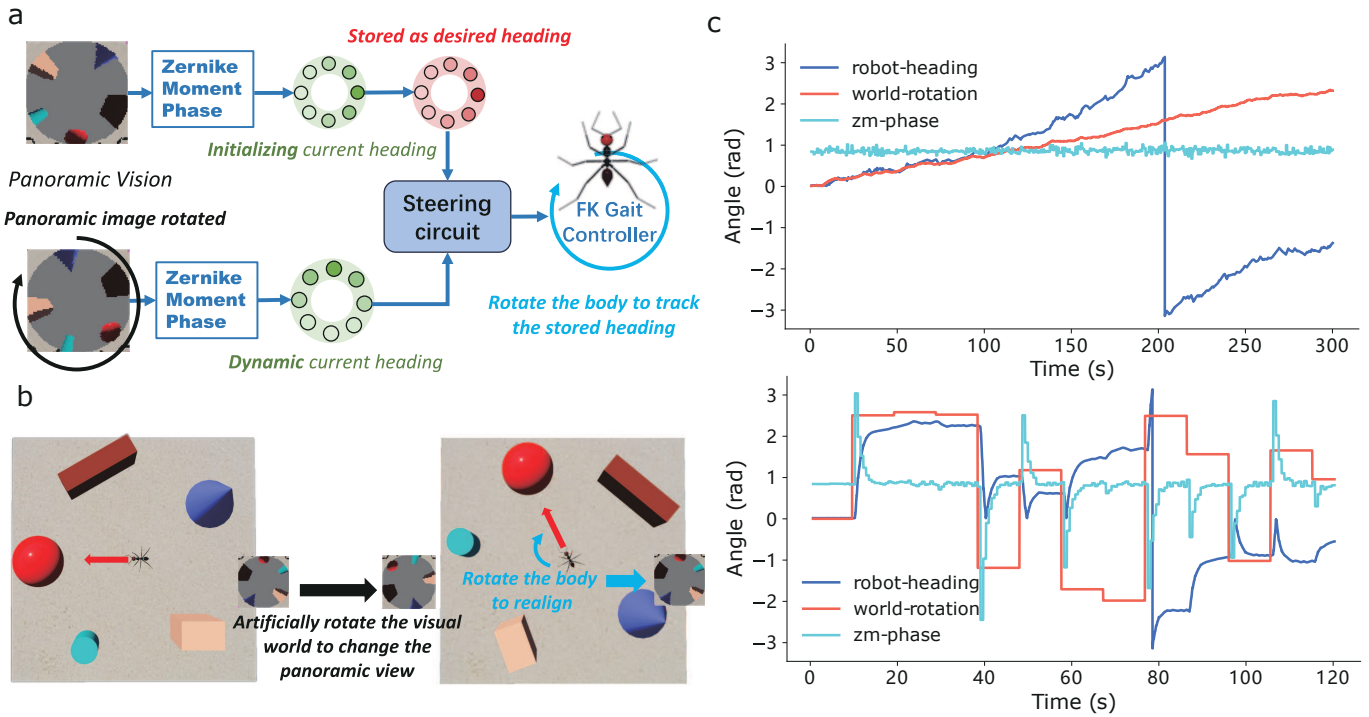

Figure 5. Visual compass using panoramic view. (*a*) Schematic diagram of the visual compass model. (*b*) Screenshot of the rotating simulated world from Webots. The rotation mode of the visual scene has two types: incremental (top of (*c*)) and jump (bottom of (*c*)). (*c*) The heading direction of the robot, the visual scene and the phase of the Zernike moment are plotted when tracking the stored direction by the Zernike moment-based visual compass.

strategy (see figure 6*g* and electronic supplementary material, video S13). As the first attempt to implement dynamic odour plume tracking in a simulated robot with realistic ant morphology and physical constraints, this case study may provide useful foundational work for future investigations into embodied olfactory-motor control.

3. Material and methods

I2Bot is built in the popular open-source robot simulator Webots [36]. The controllers of the demos presented in this paper were programmed in Python 3.9 (compatible for newer version) with packages such as *numpy*, *cv2*, *ikpy*, etc. Note that aside from Python, Webots supports multiple programming languages like Java, C/C++ and Matlab scripts. All the source code related to this project is open-sourced at Github (https://github.com/XuelongSun/I2Bot) under the MIT license.

3.1. Robot design

The morphology of a *Cataglyphis fortis* desert ant was estimated from images provided in [76] (see electronic supplementary material, figure S1). To simulate the ant body in three dimensions, we use Webots embedded geometries *sphere*, *cone* and *capsule* to model the body parts as that in [39]. As shown in electronic supplementary material, figure S1, the length of the hind leg is larger, making it distinctive as the characteristics of desert ants' leg morphology. Note that the size of the ant is scaled 100 times larger for the ease of the physics simulation within Webots.

Binocular visual sensors are placed at the position of eyes while the abstracted panoramic visual sensor is placed at the top of the ant robot's head to obtain a more ideal field of view. Olfactory sensors are mounted on the end of the antennae to mimic that of animals [47] and make it easy for robotics studies [48]. Eight tactile sensors are mounted on the tip of each leg and each antenna, which can detect three-dimensional contact force. Each joint (40 in total) has a torque sensor that could be dynamically accessed during locomotion (see figure 1). This torque feedback could be very useful in designing bio-plausible locomotion controllers like that in [49,52].

3.2. Environment construction

For visual environments, all visible objects, such as basic geometric shapes and trees used in the presented cases, are available in Webots. Vision is constructed using the camera model embedded in Webots. Additionally, simulated visual environments from previous studies on insect navigation can be easily imported into the Webots three-dimensional environment via the *Mesh* shape or *Cadshape* node. See electronic supplementary material, figure S2, for examples of visual scenes used in [27,29,68,77]. This feature allows researchers to directly obtain visual stimuli from the desired world without needing to configure a camera model, facilitating the comparison of different visual navigation models that share the same visual input.

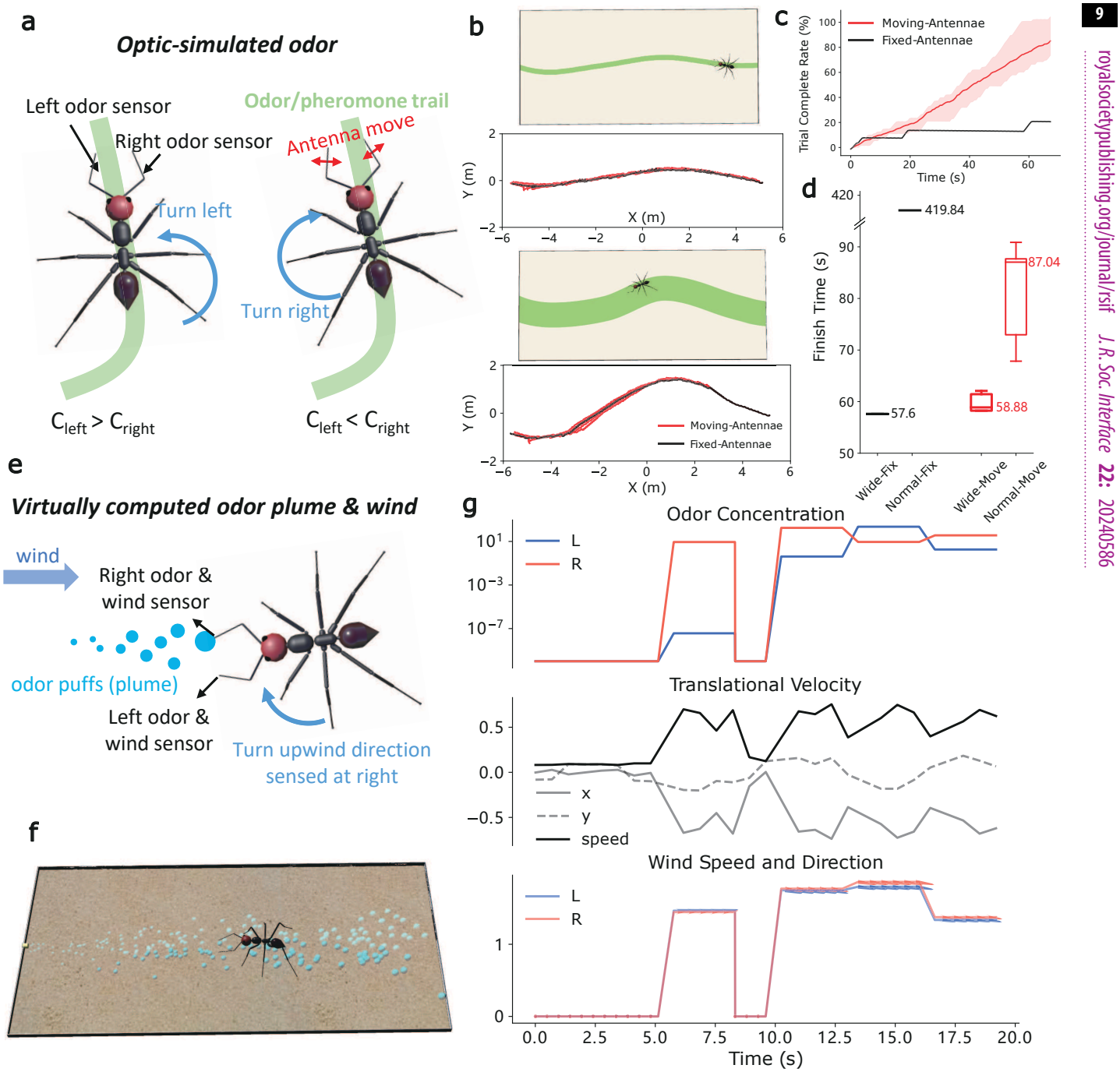

Figure 6. Olfactory-motor closed-loop control. Panels (*a–d*) depict odour trail following, while panels (*e–g*) illustrate odour plume tracking. (*a*) Schematic diagram illustrating the control strategy of the trail following behaviour. (*b*) Bird's-eye screenshots of the experiments and the corresponding trajectories of the agent with different widths of the odour trail. (*c*) Comparison of the completion rate between fixed-antenna and moving-antenna configurations. (*d*) Box plot of the finish time ($n = 5$). (*e*) Model of plume tracking. (*f*) Screenshot of the experiments in the Webots three-dimensional scene. (*g*) Perceived odour concentration (top), wind (bottom) and the moving velocity of the ant robot (middle) during one experiment.

For olfactory environments, there are two types of simulation: (i) for the odour trail, it is optically simulated as the specific texture of the floor. This texture can be drawn manually and thus allows great flexibility. (ii) For the odour plume, it is simulated by the filament-based model [78] and its Python implementation called *pompy*. This model mimics both short- and long-timescale features of odour plume evolving in a turbulent flow and has been widely used in olfactory-related studies involving insect navigation [70,79] and robot odour source localization [80].

3.3. Models

3.3.1. Forward kinematics

To simplify the gait control, we keep the ThCx and TiTa joint angles constant and denote the angles of the left three joints—ThCz, CTr and FTi to be α, β and γ, respectively. These values are determined by the hip swing (S_l with unit rad), lift swing (S_h

with unit rad) and the moving direction (−1 for backwards and 1 for forwards). To realize yaw control of the robot body, we introduced rotation configuration denoted as θ. Table 2 lists the formulae to calculate the base range of the ThCx joint R.

As different gait types share the same mechanisms, here we just describe how to use FK to generate a tripod gait, other gait could be generated with alternative leg coordination sequences. For the first half phase of a leg during the swing stage, the angles of the three joints are calculated by

$$\begin{cases} \alpha_{sw1}(k) = & -R + \alpha_0 + \dfrac{R}{S_n}k \\ \beta_{sw1}(k) = & \beta_0 + \dfrac{S_h}{S_n}k \\ \gamma_{sw1}(k) = & \gamma_0 + \dfrac{S_h}{S_n}k \end{cases} \quad , k = 0, 1, \ldots, S_n, \tag{3.1}$$

where $\alpha_0, \beta_0, \gamma_0$ is the initial angle of ThCx, CTr and FTi joint, respectively. S_n is the total time steps to lift the leg to its highest position determined by the lift swing S_h. Similarly, in the next half phase, the angles are calculated by

$$\begin{cases} \alpha_{sw2}(k) = & \alpha_0 + \dfrac{R}{S_n}k \\ \beta_{sw2}(k) = & \beta_0 + S_h - \dfrac{S_h}{S_n}k, k = 0, 1, \ldots, S_n. \\ \gamma_{sw2}(k) = & \gamma_0 + S_h - \dfrac{S_h}{S_n}k \end{cases} \tag{3.2}$$

In this phase, the leg is moved to the frontmost position (α reaches its highest value) and contacts the ground again (β and γ are set to its initial value).

For the stance phase, $\beta(k)$ and $\gamma(k)$ are kept constant (as the leg does not lift) while $\alpha(k)$ is reversed (moves from the front of the body to its back),

$$\begin{cases} \alpha_{st}(k) = & \alpha_0 + R - \dfrac{R}{S_n}k \\ \beta_{st}(k) = & \beta_0 \\ \gamma_{st}(k) = & \gamma_0 \end{cases} \quad , k = 0, 1, \ldots, S_n, S_n + 1, \ldots, 2S_n. \tag{3.3}$$

For a tripod gait, the angle of ThCx joint of FR, ML and HL leg should be α_{sw1} -> α_{sw2} ->α_{st} while that of the other three legs (i.e. FL, MR and HR) should be α_{st} -> α_{sw1} -> α_{sw2}. The angles of CTr (β) and FTi (γ) joint follow the same rule.

3.3.2. Inverse kinematics

Unlike the FK wherein the joint angles are computed directly given the leg movement parameters (i.e. hip swing S_l, lift swing S_h, etc.), when applying IK, we first calculate the positions of the leg tip at a certain time step k in swing and stance state, and then utilize the IK (with Python package *ikpy*) to compute the joint angles. The legs of the ant robot were defined by URDF files and can be read by the *ikpy* package. Specifically, the step length and step height is denoted as L and H, respectively, then for leg in the swing stage, the joint angles should be

$$[\alpha_{sw}(k), \beta_{sw}(k), \gamma_{sw}(k)] = \mathbf{ik}(Homo([0, 0, \theta - \frac{\theta}{S_n}k], [L/2 - \frac{L}{S_n}k, 0, -\frac{H}{S_n}k])) \qquad k = 0, 1, \ldots, S_n, \tag{3.4}$$

where $Homo$(**rotation**, **translation**) calculates the homogeneous matrix given the rotation and translation input and **ik()** denotes the IK function which receives the homogeneous matrix of the leg tip as parameters and returns the calculated joint angles. (This function is provided as an API in the *ikpy* package, and the specific calculations are not detailed here, as they follow standard IK processes.) θ is the rotation configuration. For the stance leg,

$$[\alpha_{st}(k), \beta_{st}(k), \gamma_{st}(k)] = \mathbf{ik}(Homo([0, 0, \frac{\theta}{S_n}k], [-L/2 + \frac{L}{S_n}k, 0, 0])) \qquad k = 0, 1, \ldots, S_n. \tag{3.5}$$

Thus, to generate a tripod gait, the angle of the ThCx joint of FR, ML and HL leg should be α_{sw} ->α_{st} while that of the other three legs (i.e. FL, MR and HR) should be α_{st} -> α_{sw}. The angles of the CTr (β) and the FTi (γ) joints follow the same rule.

3.3.3. Path integration

Path integration requires heading direction and velocity information; this is provided by the **Webots** *Supervisor* in the current implementation. One can use other modalities like vision (e.g. optic flow) to obtain this. The model of path integration is adapted from [28,29]; the output of the summed CPU1 (PFN) neurons are fed into the FK-based gait controller as follows:

$$\theta(t) = k_{PI}[\sum_{i=0}^{7} C^i_{CPU1}(t) - \sum_{i=8}^{15} C^i_{CPU1}(t)], \tag{3.6}$$

where $C^i_{CPU1}(t)$ is the membrane potential of the ith CPU1 neuron at time t. Similar with that in [28], the difference between the summed activation of left and right CPU1 neurons modifies the rotation configuration of the gait control (see table 2 for specific

Table 2. The calculation of ThCx joint range R for yaw-control of FK gait.

	left legs (FL, ML and HL)	right legs (FR, MR and HR)
$\theta \geq 0$	$S_l d(2\theta - 1)$	$S_l d$
$\theta < 0$	$S_l d(2\theta + 1)$	$-S_l d$

Table 3. Odour trail following. The threshold $T_d = 5$ and $T_o = 900$ are set empirically according to the lookup table of the DistanceSensor used. $K_d = 400$ is a constant scale factor.

sensory state	odour sensed		no odour
	$O_d < T_d$	$O_d \leq T_d$	$O^l < T_o$ **and** $O^r < T_o$
θ (degree)	0	O_d/k_d	−1 or 1 (random)
S_l (degree)	8	4	3

calculation) and thus guides the robot's turning decision via the motor scale k_{PI}. To tune the walking speed, step length S_l is computed by

$$S_l(t) = S_l^0(t) + S_l^f(t) \times (1 - \min[|\theta(t)|, 1]), \tag{3.7}$$

where the basis step length $S_l^0 = 5^\circ$ and the scale factor $S_l^f = 20^\circ$ are held constant. Thus, the step length is confined in the range of $[5^\circ, 25^\circ]$. These parameters are selected empirically based on the ant robot's performance in the designed simulation. For running multiple trials (results presented in figure 3*d*), we set the start location to be fixed at [0,0] while the initial heading varies in range $[0,2\pi]$.

3.3.4. Vision

Vision is provided through the embedded camera sensor in Webots. For panoramic view simulating, the projection mode of the camera is set to *spherical* while for monocular and binocular it is set to be *planar*. The parameters of the camera such as resolution, field of view and focal length can be customized in Webots easily through the *scene tree*.

— **Visual beaconing**. The resolution of the left and right eye camera is 74 × 19 (i.e. the image width $W_{vb} = 74$ and the image height $H_{vb} = 19$) with the horizontal and vertical field of view to be 2 rad and 0.5 rad, respectively. The motor command is calculated by the 'copy-and-shift' mechanism proposed in [17,29]. The input image will be first binaries with a given threshold (empirically selected in the range [10, 25] given that the brightness of the image is in the range [0,255]). Then the value of $shift_{vb}$ is computed by

$$shift_{vb} = \lceil |6\delta/W_{vb}| \rceil, \tag{3.8}$$

where δ is the difference between the horizontal image centre and the centre of the landmark area,

$$\delta = \begin{cases} W_{vb}^{Left} - P_l^{Left} & \text{Left monocular} \\ W_{vb}^{Right} - P_l^{Right} & \text{Right monocular} \\ \dfrac{(W_{vb}^{Left} - P_l^{Left}) + (W_{vb}^{Right} - P_l^{Right})}{2} & \text{Binocular} \end{cases}, \tag{3.9}$$

where P_l is the averaged horizontal position of the dark landmark in the left and right retina (i.e. image pixel coordinates). The desired heading is then calculated through the *copy-and-shift* mechanism wherein the current heading is copied and shifted by $shift$ amount. Then the turning value $\theta(t)$ is calculated by the steering circuit [17,28] as that in equation (3.6) but with a different motor scale of visual beacons k_{vb}. Then, the ThCx joint range R (table 2) and the hip swing $S_l(t)$ equation (3.7) of the FK gait controller are calculated to affect the locomotion.
In the multi-trial simulations, the ant robot consistently starts from the same point but with varying initial headings. Specifically, agents using the left eye view sample uniformly from the range $[0, \pi/2]$, while those using the right eye view sample from $[\pi/2, \pi]$. For binocular agents, initial headings are sampled from $[\pi/4, 3\pi/4]$.

— **Visual compass**. The resolution of the artificial panoramic vision is 72 × 72. The direction of the view is extracted by the phase information of the Zernike moment [29,68] coefficient (with order $n = 7$ and repetition $m = 1$, $\Phi_{7,1}(t)$). This Zernike phase is compared with the initially stored phase ($\Phi_{7,1}(0)$) and then the difference determines the sign of turning parameter $\theta(t)$ and the hip swing,

$$\begin{cases} \theta(t) = \text{sign}(\Phi_{7,1}(t) - \Phi_{7,1}(0)) \\ S_l(t) = |(\Phi_{7,1}(t) - \Phi_{7,1}(0))/5| \end{cases}. \tag{3.10}$$

Table 4. Comparison between different simulation tools.

	I2Bot	Hector	NeuroMechFly	NeuroMechFly2	CompoundRay
physics	✓(ODE)	✓(ODE)	✓(PyBullet)	✓(MuJoCo)	✘
vision	✓(binocular/ panoramic)	✘	✘	✓(binocular)	✓(binocular)
olfactory	✓	✘	✘	✓	✘
tactile	✓	✓	✓	✓	✘
programming language	✓(Python/Java/C/C++/ Matlab)	✓(Python)	✓(Python)	✓(Python)	✓(Python)
user interface	✓	✘	✘	✘	✘

Table 5. Roadmap for developing a community hub of simulation tools in insect neuroethology.

	now *(I2Bot currently can offer)*	*next* *(implementable immediately)*	*future* *(long-term featured goals)*
sensory	vision (binocular and panoramic); olfactory (airborne and chemical); force sensing (joint torque and tactile)	more bio-realistic vision simulation (e.g. embedded CompoundRay [85]); more precise tactile sensing with touch sensor arrays; compound odour sensing	multi-modal and real-time sensory
brain models	central complex steering circuit [28]; heading direction using ring attractor; central complex copy-and-shift [17]	mushroom bodies model for visual navigation [27]; models of the insect motor centre: lateral accessory lob (LAL) [101]; central complex multiple cues integration [17], etc.	bio-plausible neural models of insect brain
locomotion	first body model (desert ant); robotics gait control	biomimetic locomotor control (e.g. NeuroWalkNet [52]); body models of other walking insects (e.g. stick insect [83]); embedded other body model framework [102], etc.	agility of walking, flying and jumping
environment	three-dimensional visual scenes; odour plume with wind; stable odour trails; uneven terrain and walls	visual scenes reconstructed from real world; polarize light simulation; magnetic simulation; simulating multiple odours simultaneously, etc.	realistic three-dimensional and interactive environment

3.3.5. Olfactory

— **Odour trail following**. As described above, the odour trail is simulated by the texture of the floor, thus the concentration is detected by the *DistanceSensor* (note that the field type should be set to be 'infra-red') whose value is modified by a reflection factor depending on the colour, roughness and occlusion properties of the object. The detected odour concentration of the odour (returned value of the *DistanceSensor*) from the left and right antenna at time t are denoted as $O^l(t)$ and $O^r(t)$, the difference between the left and right sensed odour concentration is denoted as $O_d(t) = O^l(t) - O^r(t)$. Table 3 shows how the sensed odour concentration determines the locomotion control (i.e. determines the hip swing and rotation of the FK gait control). For multiple trial experiments, all the agents started from the same position [5,0] with identical initial heading (π).

— **Odour plume tracking**. In this simulation, the agent not only detects the odour concentration (O^l and O^r) but also the wind direction ($\mathbf{W^l} = [w_x^l, w_y^l]$ and $\mathbf{W_r} = [w_x^r, w_y^r]$). These values are computed virtually based on the filament-based model [78]. When there is no odour sensed, the agent conducts a random search around the spot (set θ to be −1 or 1 randomly and S_l to be a small value like 5°). When the odour is detected (i.e. concentration exceeds $T_o^p = 10^{-6}$), the agent compares the left and right odour concentrations, turning towards the upwind direction where a higher concentration is sensed. Specifically, the desired turning orientation is computed by $m(t) = \tan^{-1}(w_y/w_x)$. Then the step length and rotation are set to be

$$\begin{cases} \theta(t) = & \text{sign}(m(t) - h(t)) \\ S_l(t) = & \min([5 + |(m(t) - h(t))\%5|, 15]), \end{cases} \tag{3.11}$$

where $h(t)$ is the current heading of the ant robot. Note that the agent will conduct one gait loop using the parameters defined in the above equation and then go forward ($S_l = 15$, $\theta = 0$) for two gait loops.

4. Discussion

Computer simulations have proven extremely valuable in neuroethology studies of insect vision (e.g. [81,82]), brain function (e.g. [28,29]) and locomotion (e.g. [54,83]) allowing researchers to verify and adapt their hypotheses efficiently and effectively. Yet, as animal behaviour arises from the interaction of each of the above plus information from internal and external cues, new tools are required that integrate as many of these elements as possible. Moreover, for these tools to be adopted widely across this highly multi-disciplinary community they should be robust, easy to install and easy to use.

As a step towards this goal, we presented I2Bot, an open-source tool for studying the mechanisms of multi-modal and embodied insect navigation. We have provided a series of case studies that demonstrate the usability and flexibility of the proposed platform, which has the potential to accelerate research in this fast moving research field. Compared with other simulation tools (see table 4), Hector [84] and NeuroMechFly [33] primarily focus on locomotion. Additionally, I2Bot provides a flexible visual and olfactory world construction and is simple to extend with other tools. For example, CompoundRay [85] could be integrated with the camera model to generate more realistic insect visual inputs, and make use of more realistic three-dimensional environments (e.g. [86–88]). Regarding the physics engine, both the Open Dynamic Engine (ODE) and MuJoCo are popular in the robotics field, each with its own pros and cons for physics simulation (for detailed comparison, see [89,90]).

4.1. Reinforcement learning and swarm intelligence

I2Bot can also be used as a (deep) reinforcement learning (RL/DRL) tool [91–93], which is becoming a more common tool for insect neuroscience [34,79,94] and insect-inspired robotics [54,95], but requires efficient simulation to run the large number of trials involved in the optimization process. The proposed tool could provide an efficient way to conduct this kind of study. The sensory and body kinematic states of the robot can construct the *State Space*, while the motor commands sent to all available joints form the *Action Space*. Our robot, functioning as an RL *agent*, could dynamically interact with a controllable *environment*. As for *Reward*, it is scenario dependent, for example, in the visual navigation context, the distance between the agent and the desired spot could be used to form the *reward* while in the odour plume tracking case, *reward* could be determined by the sensed odour concentration. The proposed I2Bot platform offers a high variety of interaction forms that interest researchers from biology and robotics, facilitating research into the underlying mechanisms of intelligent behaviours and the training and testing of RL-based algorithms.

I2Bot is also suitable for simulating multi-agent systems, making it ideal for swarm intelligence and robotics studies [96,97]. Similar to previous studies using Webots for swarm robotics simulation [98–100], I2Bot can easily be applied to investigate similar scenarios by adding multiple ant robots (see electronic supplementary material, video S12, for an example of multiple agents simulation). This approach can lead to embodied swarm intelligence, as the body morphology and physical dynamics are integrated into this platform.

4.2. Roadmap for a community hub: simulation tools in insect neuroethology

The intention of this study was to demonstrate the opportunities that modern computer simulation tools offer to the field of insect neuroethology, taking the classic desert ant navigation problem as a representative use case. Yet, for I2Bot's maximum value to be realized will require adoption by the community to create a virtuous cycle of usage driving tool development and vice versa. We outline a roadmap of developments that could take place to enhance the tool to make it usable by the broad community of insect neuroethologists in table 5. Such extensions will allow researchers to continuously enhance the platform's capabilities and apply it to a broader range of studies in insect navigation and robotics. Our hope is to enable community hub to drive ever faster research cycles as has been realized through tool sharing in field such as machine-learning (such as FastAI [103] and MLlib [104]), robotics (like ROS [105]) and neuroscience (such as FlyWire [106] and insectBrainDB [41]). To this end, we extend an open invitation to the neuroethology community to become active contributors to this open-source project [107].

Ethics. This work did not require ethical approval from a human subject or animal welfare committee.

Data accessibility. All the source codes, model of the robot and environments are open-sourced via Zenodo [108] and Github [107].
Supplementary material is available online [109].

Declaration of AI use. We have not used AI-assisted technologies in creating this article.

Authors' contributions. X.S.: conceptualization, funding acquisition, investigation, methodology, software, validation, visualization, writing—original draft; M.M.: methodology, supervision, writing—review and editing; J.P.: funding acquisition, project administration, resources, supervision, writing—review and editing; S.Y.: conceptualization, resources, supervision, writing—review and editing.
All authors gave final approval for publication and agreed to be held accountable for the work performed therein.

Conflict of interest declaration. We declare we have no competing interests.

Funding. This research was funded by the National Natural Science Foundation of China (Grant Nos. 62206066 and 12031003) and by the Engineering and Physical Sciences Research Council, UK, under the ActiveAI grant (EP/S030964/1).

References

1. Chiel HJ, Beer RD. 1997 The brain has a body: adaptive behavior emerges from interactions of nervous system, body and environment. *Trends Neurosci*. **20**, 553–557. (doi:10.1016/s0166-2236(97)01149-1)
2. Wystrach A. 2021 Movements, embodiment and the emergence of decisions: insights from insect navigation. *Biochem. Biophys. Res. Commun*. **564**, 70–77. (doi:10.1016/j.bbrc.2021.04.114)
3. Webb B. 2001 Can robots make good models of biological behaviour? *Behav. Brain Sci*. **24**, 1033–1050; (doi:10.1017/s0140525x01000127)
4. Ijspeert AJ. 2014 Biorobotics: Using robots to emulate and investigate *agile* locomotion. *Science* **346**, 196–203. (doi:10.1126/science.1254486)
5. Franceschini N. 2014 Small brains, smart machines: from fly vision to robot vision and back again. *Proc. IEEE* **102**, 751–781. (doi:10.1109/jproc.2014.2312916)
6. Oudeyer PY. 2010 On the impact of robotics in behavioral and cognitive sciences: from insect navigation to human cognitive development. *IEEE Trans. Auton. Ment. Dev*. **2**, 2–16. (doi:10.1109/tamd.2009.2039057)
7. Webb B. 2020 Robots with insect brains. *Science* **368**, 244–245. (doi:10.1126/science.aaz6869)
8. Manoonpong P, Patanè L, Xiong X, Brodoline I, Dupeyroux J, Viollet S, Arena P, Serres JR. 2021 Insect-inspired robots: bridging biological and artificial systems. *Sensors* **21**, 7609. (doi:10.3390/s21227609)
9. Matsiko A. 2023 Taking inspiration from nature is a no-brainer. *Sci. Robot*. **8**, eadi2720. (doi:10.1126/scirobotics.adi2720)
10. Wehner R. 2019 The Cataglyphis Mahrèsienne: 50 years of Cataglyphis research at Mahrès. *J. Comp. Physiol. Neuroethol. Sens. Neural Behav. Physiol*. **205**, 641–659. (doi:10.1007/s00359-019-01333-5)
11. Menzel R, Giurfa M. 2001 Cognitive architecture of a mini-brain: the honeybee. *Trends Cogn. Sci*. **5**, 62–71. (doi:10.1016/s1364-6613(00)01601-6)
12. de Croon GCHE, Dupeyroux JJG, Fuller SB, Marshall JAR. 2022 Insect-inspired AI for autonomous robots. *Sci. Robot*. **7**, l6334. (doi:10.1126/scirobotics.abl6334)
13. Álvarez-Salvado E, Licata AM, Connor EG, McHugh MK, King BM, Stavropoulos N, Victor JD, Crimaldi JP, Nagel KI. 2018 Elementary sensory-motor transformations underlying olfactory navigation in walking fruit-flies. *eLife* **7**, e37815. (doi:10.7554/elife.37815)
14. Mangan M. 2011 Visual homing in field crickets and desert ants: a comparative behavioural and modelling study. Thesis, University of Edinburgh, UK.
15. Schilling M, Paskarbeit J, Ritter H, Schneider A, Cruse H. 2022 From adaptive locomotion to predictive action selection – cognitive control for a six-legged walker. *IEEE Trans. Robot*. **38**, 666–682. (doi:10.1109/tro.2021.3106832)
16. Wystrach A, Mangan M, Webb B. 2015 Optimal cue integration in ants. Proc. R. Soc. B **282**, 20151484. (doi:10.1098/rspb.2015.1484)
17. Sun X, Yue S, Mangan M. 2021 How the insect central complex could coordinate multimodal navigation. *eLife* **10**, e73077. (doi:10.7554/eLife.73077)
18. Schilling M, Cruse H. 2017 ReaCog, a minimal cognitive controller based on recruitment of reactive systems. *Front. Neurorobotics* **11**, 3. (doi:10.3389/fnbot.2017.00003)
19. Wehner R. 2003 Desert ant navigation: how miniature brains solve complex tasks. *J. Comp. Physiol. Neuroethol. Sens. Neural Behav. Physiol*. **189**, 579–588. (doi:10.1007/s00359-003-0431-1)
20. Heinze S. 2017 Unraveling the neural basis of insect navigation. *Curr. Opin. Insect Sci*. **24**, 58–67. (doi:10.1016/j.cois.2017.09.001)
21. Wehner R, Hoinville T, Cruse H, Cheng K. 2016 Steering intermediate courses: desert ants combine information from various navigational routines. *J. Comp. Physiol. Neuroethol. Sens. Neural Behav. Physiol*. **202**, 459–472. (doi:10.1007/s00359-016-1094-z)
22. Heinze S. 2020 Visual navigation: ants lose track without mushroom bodies. *Curr. Biol*. **30**, R984–R986. (doi:10.1016/j.cub.2020.07.038)
23. Bregy P, Sommer S, Wehner R. 2008 Nest-mark orientation *versus* vector navigation in desert ants. *J. Exp. Biol*. **211**, 1868–1873. (doi:10.1242/jeb.018036)
24. Bühlmann C, Cheng K, Wehner R. 2011 Vector-based and landmark-guided navigation in desert ants inhabiting landmark-free and landmark-rich environments. *J. Exp. Biol*. **214**, 2845–2853. (doi:10.1242/jeb.054601)
25. Legge ELG, Wystrach A, Spetch ML, Cheng K. 2014 Combining sky and earth: desert ants (*Melophorus bagoti*) show weighted integration of celestial and terrestrial cues. *J. Exp. Biol*. **217**, 4159–4166. (doi:10.1242/jeb.107862)
26. Collett M. 2012 How navigational guidance systems are combined in a desert ant. *Curr. Biol*. **22**, 927–932. (doi:10.1016/j.cub.2012.03.049)
27. Ardin P, Peng F, Mangan M, Lagogiannis K, Webb B. 2016 Using an insect mushroom body circuit to encode route memory in complex natural environments. *PLoS Comput. Biol*. (ed. J Ayers), **12**, e1004683. (doi:10.1371/journal.pcbi.1004683)
28. Stone T *et al*. 2017 An anatomically constrained model for path integration in the bee brain. *Curr. Biol*. **27**, 3069–3085.(doi:10.1016/j.cub.2017.08.052)
29. Sun X, Yue S, Mangan M. 2020 A decentralised neural model explaining optimal integration of navigational strategies in insects. elife (doi:10.1101/856153)
30. Lambrinos D, Möller R, Labhart T, Pfeifer R, Wehner R. 2000 A mobile robot employing insect strategies for navigation. *Robot. Auton. Syst*. **30**, 39–64. (doi:10.1016/s0921-8890(99)00064-0)
31. Dupeyroux J, Serres JR, Viollet S. 2019 AntBot: A six-legged walking robot able to home like desert ants in outdoor environments. *Sci. Robot*. **4**, u0307. (doi:10.1126/scirobotics.aau0307)
32. Brodland GW. 2015 How computational models can help unlock biological systems. *Semin. Cell Dev. Biol*. **47**, 62–73. (doi:10.1016/j.semcdb.2015.07.001)
33. Lobato-Rios V, Ramalingasetty ST, Özdil PG, Arreguit J, Ijspeert AJ, Ramdya P. 2022 NeuroMechFly, a neuromechanical model of adult *Drosophila melanogaster*. *Nat. Methods* **19**, 620–627. (doi:10.1038/s41592-022-01466-7)
34. Wang-Chen S, Stimpfling VA, Özdil PG, Genoud L, Hurtak F, Ramdya P. 2024 NeuroMechFly 2.0, a framework for simulating embodied sensorimotor control in adult *Drosophila*. *bioRxiv*. (doi:10.1101/2023.09.18.556649)
35. Vaxenburg R et al. 2024 Whole-body simulation of realistic fruit fly locomotion with deep reinforcement learning. bioRxiv. (doi:10.1101/2024.03.11.584515)
36. Michel O. 2004 Cyberbotics Ltd. Webots™: professional mobile robot simulation. *Int. J. Adv. Robot. Syst*. **1**, 5. (doi:10.5772/5618)
37. Xin Y, Rong X, Li Y, Li B, Chai H. 2019 Movements and balance control of a wheel-leg robot based on uncertainty and disturbance estimation method. *IEEE Access* **7**, 133265–133273. (doi:10.1109/access.2019.2940487)
38. Knüsel J, Crespi A, Cabelguen JM, Ijspeert AJ, Ryczko D. 2020 Reproducing five motor behaviors in a salamander robot with virtual muscles and a distributed CPG controller regulated by drive signals and proprioceptive feedback. *Front. Neurorobotics* **14**, 604426. (doi:10.3389/fnbot.2020.604426)
39. Ramdya P, Thandiackal R, Cherney R, Asselborn T, Benton R, Ijspeert AJ, Floreano D. 2017 Climbing favours the tripod gait over alternative faster insect gaits. *Nat. Commun*. **8**, 14494. (doi:10.1038/ncomms14494)
40. Chen Y, Grezmak JE, Graf NM, Daltorio KA. 2022 Sideways crab-walking is faster and more efficient than forward walking for a hexapod robot. *Bioinspiration Biomimetics* **17**, 046001. (doi:10.1088/1748-3190/ac6847)

41. Heinze S *et al*. 2021 A unified platform to manage, share, and archive morphological and functional data in insect neuroscience. *eLife* **10**, e65376. (doi:10.7554/eLife.65376)
42. Seelig JD, Jayaraman V. 2015 Neural dynamics for landmark orientation and angular path integration. *Nature* **521**, 186–191. (doi:10.1038/nature14446)
43. Graham P, Cheng K. 2009 Ants use the panoramic skyline as a visual cue during navigation. *Curr. Biol*. **19**, R935–7. (doi:10.1016/j.cub.2009.08.015)
44. Draft RW, McGill MR, Kapoor V, Murthy VN. 2018 Carpenter ants use diverse antennae sampling strategies to track odor trails. *J. Exp. Biol*. (doi:10.1242/jeb.185124)
45. Buehlmann C, Mangan M, Graham P. 2020 Multimodal interactions in insect navigation. *Anim. Cogn*. **23**, 1129–1141. (doi:10.1007/s10071-020-01383-2)
46. Claverie N, Buvat P, Casas J. 2023 Active sensing in bees through antennal movements is independent of odor molecule. *Integr. Comp. Biol*. **63**, 315–331. (doi:10.1093/icb/icad010)
47. Dürr V, Berendes V, Strube-Bloss M. 2022 Sensorimotor ecology of the insect antenna: active sampling by a multimodal sensory organ. In *Advances in insect physiology*, pp. 1–105, vol. **63**. Amsterdam, The Netherlands: Elsevier. (doi:10.1016/bs.aiip.2022.10.002)
48. Hoinville T, Harischandra N, Krause AF, Dürr V. 2014 Insect-inspired tactile contour sampling using vibration-based robotic antennae. In *Biomimetic and biohybrid systems lecture notes in computer science*, pp. 118–129. Cham, Switzerland: Springer International Publishing. (doi:10.1007/978-3-319-09435-9_11)
49. Schilling M, Hoinville T, Schmitz J, Cruse H. 2013 Walknet, a bio-inspired controller for hexapod walking. *Biol. Cybern*. **107**, 397–419. (doi:10.1007/s00422-013-0563-5)
50. Steingrube S, Timme M, Wörgötter F, Manoonpong P. 2010 Self-organized adaptation of a simple neural circuit enables complex robot behaviour. *Nat. Phys*. **6**, 224–230. (doi:10.1038/nphys1508)
51. Dickinson MH, Farley CT, Full RJ, Koehl MA, Kram R, Lehman S. 2000 How animals move: an integrative view. *Science* **288**, 100–106. (doi:10.1126/science.288.5463.100)
52. Schilling M, Cruse H. 2023 neuroWalknet, a controller for hexapod walking allowing for context dependent behavior. *PLoS Comput. Biol*. **19**, e1010136. (doi:10.1371/journal.pcbi.1010136)
53. Arena E, Arena P, Patane L. 2012 CPG-based locomotion generation in a Drosophila inspired legged robot. In *4th IEEE RAS & EMBS Int. Conf. on Biomedical Robotics and Biomechatronics (BioRob 2012)*, pp. 1341–1346. IEEE. (doi:10.1109/BioRob.2012.6290809)
54. Schilling M, Cruse H. 2020 Decentralized control of insect walking: a simple neural network explains a wide range of behavioral and neurophysiological results. *PLoS Comput. Biol*. **16**, e1007804. (doi:10.1371/journal.pcbi.1007804)
55. WEHNER R. 2008 The Desert ant's navigational toolkit: procedural rather than positional knowledge. *Navigation* **55**, 101–114. (doi:10.1002/j.2161-4296.2008.tb00421.x)
56. Heinze S, Narendra A, Cheung A. 2018 Principles of insect path integration. *Curr. Biol*. **28**, R1043–R1058. (doi:10.1016/j.cub.2018.04.058)
57. Kim SS, Rouault H, Druckmann S, Jayaraman V. 2017 Ring attractor dynamics in the *Drosophila* central brain. *Science* **356**, 849–853. (doi:10.1126/science.aal4835)
58. Hulse BK, Jayaraman V. 2020 Mechanisms underlying the neural computation of head direction. *Annu. Rev. Neurosci*. **43**, 31–54. (doi:10.1146/annurev-neuro-072116-031516)
59. Honkanen A, Adden A, da Silva Freitas J, Heinze S. 2019 The insect central complex and the neural basis of navigational strategies. *J. Exp. Biol.* (eds B el Jundi, A Kelber, B Webb), **222**, jeb188854. (doi:10.1242/jeb.188854)
60. Collett M, Chittka L, Collett TS. 2013 Spatial memory in insect navigation. *Curr. Biol*. **23**, R789–800. (doi:10.1016/j.cub.2013.07.020)
61. Freas CA, Spetch ML. 2023 Varieties of visual navigation in insects. *Anim. Cogn*. **26**, 319–342. (doi:10.1007/s10071-022-01720-7)
62. Collett TS, Baron J. 1994 Biological compasses and the coordinate frame of landmark memories in honeybees. *Nature* **368**, 137–140. (doi:10.1038/368137a0)
63. Buehlmann C, Wozniak B, Goulard R, Webb B, Graham P, Niven JE. 2020 Mushroom bodies are required for learned visual navigation, but not for innate visual behavior, in ants. *Curr. Biol*. **30**, 3438–3443.(doi:10.1016/j.cub.2020.07.013)
64. Zeil J, Hofmann MI, Chahl JS. 2003 Catchment areas of panoramic snapshots in outdoor scenes. *J. Opt. Soc. Am. Opt. Image Sci. Vis*. **20**, 450–469. (doi:10.1364/josaa.20.000450)
65. Wystrach A, Beugnon G, Cheng K. 2011 Landmarks or panoramas: what do navigating ants attend to for guidance? *Front. Zool*. **8**, 21. (doi:10.1186/1742-9994-8-21)
66. Collett TS. 2008 Insect navigation: visual panoramas and the sky compass. *Curr. Biol*. **18**, R1058–61. (doi:10.1016/j.cub.2008.10.006)
67. Stürzl W, Möller R. 2007 An insect-inspired active vision approach for orientation estimation with panoramic images. In International Work—Conf. on the Interplay between Natural and Artificial Computation, pp. 61–70. Berlin, Germany: Springer. (doi:10.1007/978-3-540-73053-8_6)
68. Stone T, Mangan M, Wystrach A, Webb B. 2018 Rotation invariant visual processing for spatial memory in insects. *Interface Focus* **8**, 20180010. (doi:10.1098/rsfs.2018.0010)
69. Philippides A, Baddeley B, Cheng K, Graham P. 2011 How might ants use panoramic views for route navigation? *J. Exp. Biol.* **214**, 445–451. (doi:10.1242/jeb.046755)
70. Cardé RT, Willis MA. 2008 Navigational strategies used by insects to find distant, wind-borne sources of odor. *J. Chem. Ecol*. **34**, 854–866. (doi:10.1007/s10886-008-9484-5)
71. Steck K, Hansson BS, Knaden M. 2009 Smells like home: desert ants, *Cataglyphis fortis*, use olfactory landmarks to pinpoint the nest. *Front. Zool*. **6**, 5. (doi:10.1186/1742-9994-6-5)
72. Steele TJ, Lanz AJ, Nagel KI. 2023 Olfactory navigation in arthropods. *J. Comp. Physiol. Neuroethol. Sens. Neural Behav. Physiol*. **209**, 467–488. (doi:10.1007/s00359-022-01611-9)
73. Reddy G, Murthy VN, Vergassola M. 2022 Olfactory sensing and navigation in turbulent environments. *Annu. Rev. Condens. Matter Phys*. **13**, 191–213. (doi:10.1146/annurev-conmatphys-031720-032754)
74. Traner M, Raman B. 2023 Dynamic walking behavior during odor trail-following in locusts. bioRxiv. (doi:10.1101/2023.02.22.529569)
75. Matheson AMM, Lanz AJ, Medina AM, Licata AM, Currier TA, Syed MH, Nagel KI. 2022 A neural circuit for wind-guided olfactory navigation. Nat. Commun. **13**, 4613. (doi:10.1038/s41467-022-32247-7)
76. Wehner R. 1983 'Taxonomie, Funktionsmorphologie und Zoogeographie der Saharischen Wüstenameise Cataglyphis fortis (Forel 1902). *Stat. Nov. Senck. Biol.* **64**, 89–132.
77. Baddeley B, Graham P, Husbands P, Philippides A. 2012 A model of ant route navigation driven by scene familiarity. *PLoS Comput. Biol*. **8**, e1002336. (doi:10.1371/journal.pcbi.1002336)
78. Farrell JA, Murlis J, Long X, Li W, Carde R. 2002 Filament-based atmospheric dispersion model to achieve short time-scale structure of odor plumes. *Env. Fluid Mech*. **2**, 143–169. (doi:10.21236/ada399832)
79. Singh SH, van Breugel F, Rao RPN, Brunton BW. 2023 Emergent behaviour and neural dynamics in artificial agents tracking odour plumes. *Nat. Mach. Intell*. **5**, 58–70. (doi:10.1038/s42256-022-00599-w)
80. Kowadlo G, Russell RA. 2008 Robot odor localization: a taxonomy and survey. *Int. J. Robot. Res*. **27**, 869–894. (doi:10.1177/0278364908095118)
81. Wystrach A, Dewar A, Philippides A, Graham P. 2016 How do field of view and resolution affect the information content of panoramic scenes for visual navigation? A computational investigation. *J. Comp. Physiol. Neuroethol. Sens. Neural Behav. Physiol*. **202**, 87–95. (doi:10.1007/s00359-015-1052-1)
82. Gkanias E, Risse B, Mangan M, Webb B. 2019 From skylight input to behavioural output: a computational model of the insect polarised light compass. *PLoS Comput. Biol*. **15**, e1007123. (doi:10.1371/journal.pcbi.1007123)
83. Rosano H, Webb B. 2006 The control of turning in real and simulated stick insects. In *Int. Conf. on Simulation of Adaptive Behavior*, pp. 150–161. Berlin, Germany: Springer. (doi:10.1007/11840541_13)
84. Dürr V *et al*. 2019 Integrative biomimetics of autonomous hexapedal locomotion. *Front. Neurorobotics* **13**, 88. (doi:10.3389/fnbot.2019.00088)
85. Millward B, Maddock S, Mangan M. 2022 CompoundRay, an open-source tool for high-speed and high-fidelity rendering of compound eyes. *eLife* **11**, e73893. (doi:10.7554/eLife.73893)

86. Risse B, Mangan M, Stürzl W, Webb B. 2018 Software to convert terrestrial LiDAR scans of natural environments into photorealistic meshes. *Environ. Model. Softw*. **99**, 88–100. (doi:10.1016/j.envsoft.2017.09.018)
87. Murray T, Zeil J. 2017 Quantifying navigational information: the catchment volumes of panoramic snapshots in outdoor scenes. *PLoS One* **12**, e0187226. (doi:10.1371/journal.pone.0187226)
88. Stürzl W, Boeddeker N, Dittmar L, Egelhaaf M. 2010 Mimicking honeybee eyes with a 280° field of view catadioptric imaging system. *Bioinspiration Biomimetics* **5**, 036002. (doi:10.1088/1748-3182/5/3/036002)
89. Erez T, Tassa Y, Todorov E. 2015 Simulation tools for model-based robotics: comparison of Bullet, Havok, MuJoCo, ODE and PhysX. In *2015 IEEE Int. Conf. on Robotics and Automation (ICRA)*, *Seattle, WA*, pp. 4397–4404. IEEE. (doi:10.1109/ICRA.2015.7139807)
90. Körber M, Lange J, Rediske S, Steinmann S, Glück R. 2021 Comparing popular simulation environments in the scope of robotics and reinforcement learning. *arXiv.* (doi:10.48550/arXiv.2103.04616)
91. van Otterlo M, Wiering M. 2012 Reinforcement learning and Markov decision processes. In *Adaptation, learning, and optimization reinforcement learning*, pp. 3–42. Berlin, Germany: Springer. (doi:10.1007/978-3-642-27645-3_1)
92. Li Y. 2017 Deep reinforcement learning: an overview. arXiv. (doi:10.48550/arXiv.1701.07274)
93. Sutton RS. 2018 Reinforcement learning: an Introduction. In *Bradford book*, pp. 1–3. Cambridge, MA: MIT Press.
94. Lochner S, Honerkamp D, Valada A, Straw AD. 2024 Reinforcement learning as a robotics-inspired framework for insect navigation: from spatial representations to neural implementation. *Front. Comput. Neurosci*. **18**, 1460006. (doi:10.3389/fncom.2024.1460006)
95. Azayev T, Zimmerman K. 2020 Blind hexapod locomotion in complex terrain with gait adaptation using deep reinforcement learning and classification. *J. Intell. Robot. Syst*. **99**, 659–671. (doi:10.1007/s10846-020-01162-8)
96. Dorigo M, Birattari M, Garnier S, Hamann H, de Oca MM, Solnon C, Stützle T. 2007 Swarm intelligence. Scholarpedia **2**, 1462. (doi:10.4249/scholarpedia.1462)
97. Brambilla M, Ferrante E, Birattari M, Dorigo M. 2013 Swarm robotics: a review from the swarm engineering perspective. *Swarm Intell*. **7**, 1–41. (doi:10.1007/s11721-012-0075-2)
98. Khaldi B, Cherif F. 2015 An overview of swarm robotics: swarm intelligence applied to multi-robotics. *Int. J. Comput. Appl*. **126**, 31–37. (doi:10.5120/ijca2015906000)
99. Newton AL, Nehaniv CL, Dautenhahn K. 2003 The robot in the swarm: an investigation into agent embodiment within virtual robotic swarms. In *European Conf. on Artificial Life*, pp. 829–838. Berlin, Germany: Springer. (doi:10.1007/978-3-540-39432-7_89)
100. Raoufi M, Turgut AE, Arvin F. 2019 Self-organized collective motion with a simulated real robot swarm. In *Towards Autonomous Robotic Systems: 20th Annual Conf., TAROS 2019*, London, UK, pp. 263–274. Cham, Switzerland: Springer. (doi:10.1007/978-3-030-23807-0_22)
101. Adden A, Stewart TC, Webb B, Heinze S. 2022 A neural model for insect steering applied to olfaction and path integration. *Neural Comput*. **34**, 2205–2231. (doi:10.1162/neco_a_01540)
102. Arreguit J, Ramalingasetty ST, Ijspeert A. 2024 FARMS: framework for animal and robot modeling and simulation. *BioRxiv.* (doi:10.1101/2023.09.25.559130)
103. Howard J, Gugger S. 2020 Fastai: a layered API for deep learning. *Information* **11**, 108. (doi:10.3390/info11020108)
104. Meng X, Bradley J, Yavuz B, Sparks E, Venkataraman S, Liu D, Freeman J. 2016 Mllib: machine learning in Apache Spark. J. Mach. Learn. Res. **17**, 1–7.
105. Cousins S, Gerkey B, Conley K, Garage W. 2010 Sharing software with ROS [ROS topics]. *IEEE Robot. Autom. Mag*. **17**, 12–14. (doi:10.1109/mra.2010.936956)
106. Dorkenwald S *et al*. 2022 FlyWire: online community for whole-brain connectomics. *Nat. Methods* **19**, 119–128. (doi:10.1038/s41592-021-01330-0)
107. Sun X. 2024 I2Bot. GitHub. https://github.com/XuelongSun/I2Bot
108. Sun X. 2024 I2Bot: An open-source tool for simulating multi-modal and embodied insect navigation. Zenodo. (doi:10.5281/zenodo.14050937)
109. Sun X, Mangan M, Yue S, Peng J. 2024 Supplementary material from: I2Bot: an open-source tool for multi-modal and embodied simulation of insect navigation. Figshare. (doi:10.6084/m9.figshare.c.7596418)